Carbazole ligands as c-myc G-quadruplex binders

Agata Głuszyńska, Bernard Juskowiak, Martyna Kuta-Siejkowska, Marcin Hoffmann, Shozeb Haider

PII: S0141-8130(17)35211-X
DOI: doi:10.1016/j.ijbiomac.2018.03.135
Reference: BIOMAC 9357

To appear in:

Received date: 27 December 2017
Revised date: 16 March 2018
Accepted date: 21 March 2018

Please cite this article as: Agata Głuszyńska, Bernard Juskowiak, Martyna Kuta-Siejkowska, Marcin Hoffmann, Shozeb Haider , Carbazole ligands as c-myc G-quadruplex binders. The address for the corresponding author was captured as affiliation for all authors. Please check if appropriate. Biomac(2017), doi:10.1016/j.ijbiomac.2018.03.135

Carbazole ligands as c-myc G-quadruplex binders

Agata Głuszyńska[a,*], Bernard Juskowiak[a], Martyna Kuta-Siejkowska[b], Marcin Hoffmann[b], Shozeb Haider[c]

[a]Laboratory of Bioanalytical Chemistry, Faculty of Chemistry, Adam Mickiewicz University, Poznań 61-614, Umultowska Street 89b, Poland
[b]Laboratory of Quantum Chemistry, Faculty of Chemistry, Adam Mickiewicz University, Poznań 61-614, Umultowska Street 89b, Poland
[c]Department of Pharmaceutical and Biologial Chemistry, School of Pharmacy, University College London, London WC1N 1AX, UK

Key words: c-myc G–quadruplex, Pu22, carbazole derivatives, spectroscopy, molecular modeling

Abstract

The interactions of c-myc G–quadruplex with three carbazole derivatives were investigated by UV-Vis spectrophotometry, fluorescence, CD spectroscopy, and molecular modeling. The results showed that a combination of carbazole scaffold functionalized with ethyl, triazole and imidazole groups resulted in stabilization of the intramolecular G-quadruplex formed by the DNA sequence derived from the NHE III_1 region of c-myc oncogene (Pu22). Binding to the G-quadruplex Pu22 resulted in the significant increase in fluorescence intensity of complexed ligands **1**-**3**. All ligands were capable of interacting with G4 DNA with binding stoichiometry indicating that two ligand molecules bind to G-quadruplex with comparable affinity, which agrees with binding model of end-stacking on terminal G-tetrads.

1. Introduction

G-quadruplexes (G4) are DNA structures that have been found in guanine-rich regions of the human genome such as human telomeres [1-4], as well as in promoter regions of certain oncogenes, including c-myc [5-7], c-kit [8,9], bcl-2 [10,11] or RET [12,13]. It has been reported that G-quadruplexes found in many human oncogene promoter regions form three-tetrad intramolecular parallel-stranded G-quadruplex structures [5,6,13-19]. The four-stranded structures of G-quadruplexes are formed by multiple vertically stacked guanine quartets (G-tetrads), which are stabilized by Hoogsteen hydrogen bonds, monovalent cations such as potassium and sodium, and can be further stabilized by specific ligands [20-24]. In the group of proto-oncogenes, the most extensively studied and the best-characterized is the c-myc oncogene, involved in cellular proliferation and cell growth, which may also affect inhibition of the apoptosis. The overexpression of c-myc can be caused by different mechanisms of transcription and is associated with a wide range of human cancers, such as lung, breast, colon, cervix, or leukemia [2,25-29]. In the nuclear hypersensitivity element III_1 (NHE III_1), the guanine-rich DNA sequence containing 27 base-pairs located 142-115 bp upstream from the P1 promoter of c-myc, controls 80-90% of the c-myc transcription level [7,30-32]. A large number of G-quadruplex stabilizing ligands as promising precursors for drug development in anticancer therapy have been described. There are many ligands capable of inducing and stabilizing G4 formation in telomeric DNA, which have shown to inhibit telomerase activity [23,24,33-47].
Also a large number of small molecules are potent G-quadruplex ligands that exhibit anti-proliferative activity in cells [39,48]. Several small molecules, for example cyclic naphthalene diimide derivative [43], cationic porphyrins [2,49-52] and pentaheteroaryls [53], quinacridines [52], PIPER [52], quarfloxin [54], methylene blue derivatives [55], fonsecin B [56], berberine derivatives

[57], carbazoles [58,59], quindoline derivatives [6,60], platinum [61-64] and cobalt [65] complexes, bisquinoline-pyrrole oligoamide [66], indolylmethyleneindanones [67], amido phthalocyanines [68], bisbenzimidazole carboxamide derivatives of pyridine, 1,8-naphthyridine, and 1,10-phenanthroline [69], or perylene and coronene derivatives [70], have been identified to bind and stabilize G-quadruplex structures in the c-myc promoter region. Carbazole derivatives are very interesting compounds because of their biological and photophysical properties. They are able to target DNA structures, some of which have potential for development into anticancer drugs [71,72]. Imidazole and triazole groups, as well as carbazole-based compounds, play an important role in medicinal chemistry, because many of them exhibit various biological properties - antibacterial, antifungal, antiinflammatory, antiparasitic, anticancer, antiviral [73-75].

In this study we present the stability and interaction of three carbazole ligands with G-quadruplex formed by a sequence corresponding to Pu22 region of c-myc NHE III_1. Pu22 is the modified mycPu22, the wild-type 22-mer G-rich sequence of the c-myc NHE III_1 that forms a parallel intramolecular G-quadruplex in the physiological K^+ solution. This structure was resolved by NMR method after modification of mycPu22 at the 14 and 23 positions (G-to-T substitutions) [6].

2. Materials and methods

2.1. Ligands

Carbazole derivative **1** was synthesized following the published procedure with some modifications [76,77]. Carbazole derivatives **2** and **3** were synthesized by the method reported in our previous paper [78]. The purity of ligands was examined by the HPLC technique. These studies were performed on a Waters HPLC system 1525 equipped with a Photodiode Array detector 2998 and a fluorescence detector 2475, a Breeze interface. A Symmetry®C18 column (d_p = 3.5 µm, 75x4.6 mm i.d.) (Waters) was used with isocratic elution (70% MeOH and 30% 10 mM NaCl, flow rate 1 ml min^{-1}).

2.2. Oligonucleotide

The quadruplex-forming 22-mer deoxyribonucleotide with c-myc sequence of 5'-TGAGGGTGGGTAGGGTGGGTAA-3' (Pu22) was purchased from Genomed (Poland) and was used without further purification. The strand concentration was determined at 260 nm at 85 °C using extinction coefficient of 254600 M^{-1} cm^{-1} as calculated from the published values of molar absorptivities of nucleotides [79]. Before using, the oligonucleotide solution was heated at 90 °C for 5 min and subsequently allowed to slow cooling to room temperature, and stored at 4 °C overnight. Tris Base (CAS Number 77-86-1) and Tris HCl (CAS Number 1185-53-1) were obtained from Aldrich Chemical Co. and used as received. A Milli-Q filtered water (Millipore Co.) was used throughout.

2.3. Absorption spectroscopy

The absorption spectra were recorded on a Cary-100 spectrophotometer (Agilent Technologies Australia) in the 300–750 nm range at 25 °C. All of the measurements were carried out using a 10 mm quartz cell. UV–Vis absorption titrations were carried out by the stepwise addition of 1 µl aliquots of 713 µM/strand of G4 DNA Pu22 solution to a cell containing 1000 µl of 6 µM ligand. Three minutes was the equilibration time after each DNA addition. All measurements were performed in a 10 mM Tris–HCl buffer (pH 7.2) containing 150 mM KCl.

2.4. Fluorescence spectroscopy

The fluorescence measurements were carried out using a Jasco FP 8200 spectrofluorimeter. The cell compartments were thermostated at 25ºC. All of the measurements were carried out using a 10 mm quartz cell. The fluorescence spectra were collected from 515 to 750 nm with both excitation and emission slits being 5 nm. Fluorescence titrations were carried out by the stepwise addition of 1 µl aliquots of 367 µM/strand of G4 DNA Pu22 solution to a cell containing 1000 µl of 2 µM ligand. Three minutes was the equilibration time after each DNA addition followed by emission spectrum recording. Excitation wavelength depended on the absorption spectrum of the ligand. All measurements were performed in a 10 mM Tris–HCl buffer (pH 7.2) containing 150 mM KCl.
The spectra in FID experiment and fluorescence titration experiments with thiazole orange (TO) as a fluorescent probe were recorded in the spectral range of 490–750 nm with excitation wavelength at 480 nm and excitation/emission slits set at 10 nm. In FID experiment the mixture of pre-folded oligonucleotide (0.25 µM) and TO (0.5 µM) was allowed to equilibrate for 10 min prior the stepwise addition of small portions of ligand **3**. In titration experiments the solution of pre-folded oligonucleotide (0.25 µM) and carbazole ligand **3** (0.25 µM or 0.5 µM) was allowed to equilibrate for 10 min prior the stepwise addition of small portions of TO. The sample solution was incubated for 3 min before recording the spectrum to allow equilibration.

2.5. Ligand - Pu22 Binding Study

Binding data obtained from spectrophotometric and spectrofluorimetric titrations were analyzed according to the method of Scatchard and/or using Benesi-Hildebrand transformation [80-82]. Experiments were carried out in the same manner - after each G4 DNA addition, the titrated solution was incubated for 3 minutes followed by the UV-Vis or fluorescence spectrum measurement. The titration was continued until only small changes in the absorption or fluorescence spectra were observed upon successive addition of Pu22.

The Scatchard model is represented by the equation:

$$\frac{r}{[L]} = Kn - Kr \qquad (1)$$

where r is the binding ratio (defined as a ratio of bound ligand over the total concentration of DNA binding sites), [L] is the concentration of free ligand while K and n correspond to the association constant of G4/ligand complex and the number of bound ligand molecules per G-quadruplex, respectively.

The method of Benesi-Hildebrand, used to estimate the value of nK_b, is represented by the equations (2, 3) that describe the n-site ligand binding model:

$$\frac{cL}{A\text{-}Ao} = \frac{cL}{Am\text{-}Ao} + \frac{cL}{(Am\text{-}Ao)nKb} x \frac{1}{cG4\,DNA} \qquad (2)$$

$$\frac{1}{F\text{-}Fo} = \frac{1}{Fm\text{-}Fo} + \frac{1}{(Fm\text{-}Fo)nKb} x \frac{1}{cG4\,DNA} \qquad (3),$$

where cL is concentration of free ligand, Ao is the absorbance of ligand in the absence of G4 DNA, A is the absorbance recorded in the presence of added G4 DNA, Am is absorbance in presence of added [G4 DNA]max, Fo is the fluorescence of ligand in the absence of G4 DNA, F is the fluorescence recorded in the presence of added G4 DNA, Fm is fluorescence in presence of added [G4 DNA]max, and n is the number of bound ligand molecules per G-quadruplex, K_b is the binding constant.

2.6. Circular dichroism

Circular dichroism (CD) spectra were recorded on a Jasco J-810 spectropolarimeter (Jasco, Japan), in the spectral range from 210 to 600 nm with 500 nm/min scan speed and bandwidth of 1 nm. Spectra were recorded in quartz cuvettes of 1 cm path length and averaged from 3 scans. Measurements with oligonucleotide were performed at 25 °C in a 10 mM Tris–HCl buffer (pH 7.2) containing 100 mM KCl. Concentration of 22-mer oligonucleotide Pu22 was 5 μM / strand. Ligands were added to G4 DNA solution at increasing concentration from 0.1 to 5 molar equivalents.

In the melting studies, the temperature of the samples were maintained by a Jasco Peltier temperature controlled cell holder. The melting profiles of G4: the c-myc G-quadruplex samples were prepared by heating the 2 μM oligonucleotide solution in 10 mM Tris HCl buffer, pH 7.2, and 25 mM or 150 mM KCl at 90 °C for 5 min followed by slow cooling, and storing at 4 °C overnight. The melting profiles were recorded in the absence and presence of 3 eq of ligands **1**-**3** in 10–95°C range with 1°C/min scan speed. Also the melting profiles of 2 μM solution c-myc oligonucleotide in 10 mM Tris HCl buffer (pH 7.2) were recorded in the absence and presence of 3 eq of ligands **1**-**3** in 95-10°C range with 1°C/min scan speed. All experiments were carried out using quartz cuvettes with a 10 mm optical path. Data were collected at 265 nm. Typically three replicate experiments were performed, and average values are reported.

2.7. Molecular modeling studies

The design protocol we used was based on the combined use of docking and molecular dynamics simulations, in which the ligand, the target and the solvent were described by an atomistic force field. In particular, we first used the docking calculations in order to establish the favourable position of the ligands. We then performed molecular dynamics simulations to check the stability of studied complexes. The final quality measure was the average value of the scoring function on a long molecular dynamics simulation. The Pu22 sequence from c-myc (PDB ID: 2L7V, 5'-TGAGGGTGGGTAGGGTGGGTAA-3') promoter region was chosen as a model for G-quadruplex for both molecular docking of the ligands and molecular simulations [6]. We used the DNA modifications to AMBER force field for system modeling [83-87]. The topologies were generated by tleap program in AMBERTOOLS software package [88].

2.7.1. Ligand docking and modeling

The quindoline ligands were extracted from the crystal structure (PDB id:2L7V) and carbazole ligands **1**-**3** were re-docked in the same position. The parameters used in obtaining the redocked conformation were used to dock other ligands. ICM lig-edit module was used to generate ligand **1**, **2** and **3**. Docking grid was centered on both ends of G-quadruplex structure, taking into account all residues around existing ligand (quindoline). For each compound we used The Atomic Property Fields superposition template method to obtain the most reliable results [89]. Indoline skeleton was used as a template because of its common substructure in both re-docked and carbazole ligands. The G-tetrads were restrained in their original conformations throughout the docking procedures. The final conformations of the docked complexes were used to carry out molecular dynamics simulations.

2.7.2. Molecular dynamics simulations

The crystal structure of intramolecular parallel-stranded G-quadruplex formed from *c-myc* gene promoter region 5'-TGAGGGTGGGTAGGGTGGGTAA-3' (PDB id:2L7V) was used as the

starting structure for the simulation. 2 K^+ ions were added in the central channel between the quartets. The structure was explicitly solvated with TIP3PBOX water molecules in a periodic box whose boundaries extended at least 10 Å from any solute atom. Additional K^+ counter ions were added to the system to neutralize the charge on the quadruplex backbone. The counterions were automatically placed, using the Coulombic potential, into the most negative locations by the LEAP program. Periodic boundary conditions were applied to avoid the edge effect. The particle mesh Ewald (PME) method was employed to calculate long-range electrostatic interactions. The AMBER ff99sb force field [84] with parmbsc1 [85] and $\chi_{OL3+OL15}$ [86,87] modifications were applied for G-quadruplexes, ions, and water molecules. The ligands were parameterised using the GAFF force field [90]. A 10 ns MD equilibration was performed in which system was restrained while solvent and ions were allowed to equilibrate. The production run with no restraints on the system was run for 1 μs (1000ns) simulations using the ACEMD molecular dynamics engine [91]. The trajectories were analyzed using the g_rmsd and g_rmsf module available in the GROMACS suite (www.gromacs.org) [92], and visualized by means of the VMD program [93] and ICM-Pro Molsoft molecular modelling package [94].

2.7.3. Interactions and stability analysis

To assess the stability of the complexes we calculated RMSD (Root-mean-square-deviation) and RMSF (Root-mean-square fluctuations) value through trajectory by using GROMACS package. RMSD value is often used to evaluate the stability of complex during simulations. The result allows the evaluation of the conformational freedom of loops and G-tetrad and checks the influence of the ligands on conformational freedom of the quadruplex structure. AutoDock Vina [95] program were used to estimate the binding affinity with using 'score only' options. Program allows the calculation of the ligand – receptor affinity at predetermined time intervals of the simulation. The scoring function that we used was mostly inspired by X-score. As a results we obtained graph of energy dependence on time (Fig. 10) [96].

2.7.4. Clustering

Clustering is a useful task to group members of structure, which are similar to each other into cluster. To identify the number of structure into clusters it is necessary to use differentiating parameters. In our protocol we used RMSD (root mean square deviation) to identify structural clusters from a trajectory. RMSD parameter enables to calculate the pairwise distances measured as coordinates between structures are defined by a cut-off value reflecting the range of conformations and their relative populations. The algorithm generates the most representative centroids structure for each cluster and then gives an RMSD for each structure in the trajectory with respect to each identified cluster. The MMTSB toolkit code was used with a cut-off of 3.0 Å for all frames from trajectory, which were extracted at a time interval of 40 ps for a total of 25 000 frames [85].

3. Results and discussion

3.1. Ligands

Our research group identified carbazole derivatives **1-3**, as potent G-quadruplex stabilizers [78,97,98]. All carbazole cationic ligands were used in our study in the form of iodide salts. As shown in Fig. 1, they possess single cationic charge on benzothiazolium moiety, varied length of linker R (2 or 4 carbon atoms) attached to the nitrogen atom and to the substituent with different electronic nature (an azole rings against aliphatic ethyl chain). Azole moieties such as imidazole [73,99-101] and triazole [74,75,102-104] are important pharmacophores occurring widely in various

types of pharmaceuticals that possess a variety of pharmacological activities. Replacement of the imidazole substituent with triazole may cause a reduction or an increase in bioactivity [105]. Also a combination of two or more types of pharmacophores in one molecule can increase bioactivity [74,102]. All the ligand samples were dissolved in DMSO for stock solution 1.5 mM and stored at 4 °C under light protection before use. These compounds are stable for several months, which was controlled using UV-Vis and fluorescence techniques.

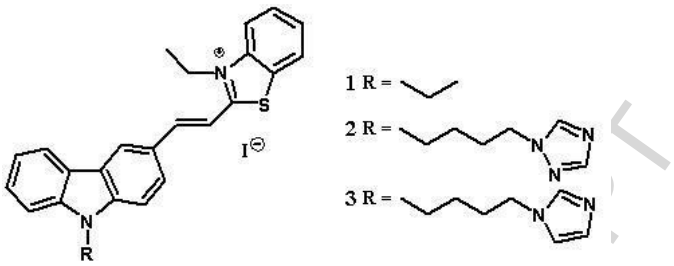

Fig. 1. Structures of carbazole ligands **1-3**.

To investigate the effect of these carbazole derivatives on parallel intramolecular G-quadruplex formed in Pu22 region of c-myc protooncogene (Fig. 2) [6], UV-Vis absorption, fluorescence and circular dichroism (CD) techniques, as well as molecular modeling were used.

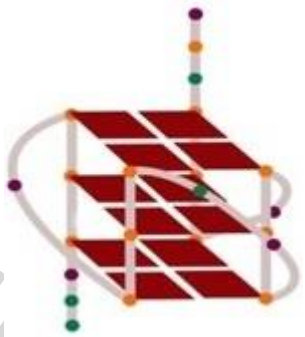

Fig. 2. Structure of G-quadruplex formed by Pu22 (5'-TGAGGGTGGGTAGGGTGGGTAA-3') [PDB ID: 2L7V]. Orange ball = guanine, purple ball = thymine, green ball = adenine.

3.2. UV-Vis absorption spectroscopy

The ability of ligands to interact with c-myc G-quadruplex DNA was first studied by spectrophotometric titration experiments. Carbazole ligands **1-3** form strong complexes with c-myc Pu22 sequence as indicated by the visible absorption spectra of carbazole ligands in the absence and presence of G-quadruplex (Figs. 3A, S1). The long wavelength maxima of absorption spectra, characteristic for carbazole chromophore conjugated with benzothiazolim system via double bond C=C, changed dramatically upon addition of G4 DNA, and the bathochromic shifts ($\Delta\lambda$ = 52-57 nm) and initial hypochromicity (24-30 %) followed by hyperchromicity (14-32 %) were observed (Table 1). High values of red shifts and hypochromicity indicate strong stacking interactions between carbazole ligands and G-tetrads. The dominant loop or groove binding is less likely, because it would not impose such large changes in UV-Vis spectra. This conclusion is confirmed by CD and molecular modeling studies (vide infra).

Table 1
Spectral effects for the ligands **1–3** bound to G4 DNA (4.2.1 in Experimental).

Ligands	$\Delta\lambda_{max}$ [nm][a]	Hypochromicity [%][b]	Hyperchromicity [%][b]
1	57	30	32
2	52	24	14
3	52	28	18

[a]$\Delta\lambda$ bathochromic shift.
[b]Hypochromicity and hyperchromicity were measured at λ_{max}. The hypo- and hyperchromicity percentages were calculated using following equations: %Hypo = $[(A_f-A_{b,min})/A_f]$x100 and %Hyper= $[(A_{b,max}-A_{b,min})/ A_{b,max}]$x100, where A_f, $A_{b,min}$, $A_{b,max}$ are the absorbances of free ligand, bound ligand with absorbance minimum, and bound ligand with absorbance maximum (excess of G4), respectively.

The Pu22/**1** complex shows the largest decrease in absorbance (hypochromicity of 30 %), although %Hypo values for all ligands are comparable (24-30 %). This indicates that the carbazole ligands/G-tetrad stacking interactions in these complexes are similar. For the typical intercalation binding modes red shifts (at least 15 nm) and large hypochromicities (at least 35%) are generally observed. However, these values are determined for long pieces of duplex DNA, where intercalation dominates but end-stacking interaction is not important [106]. In addition, no sharp isosbestic points were observed. Probably this is the result of multiple conformations for the G-quadruplex and G-quadruplex-ligand complexes [107]. UV-Vis absorption measurements suggested the two-step complex formation between ligands and G-quadruplex. At lower G4/ligand ratios, the positively charged ligand may stack onto the phosphate groups of G-quadruplex surface as a result of electrostatic attraction. Subsequent redistribution of the ligand molecules at higher G4 concentrations is responsible for hyperchromic effect and the interaction of ligand-G4 in another binding mode, namely through the end-stacking interactions. [107-110]. The spectrophotometric titration results show a trend that is consistent with the binding scores predicted by molecular modeling (vide infra).

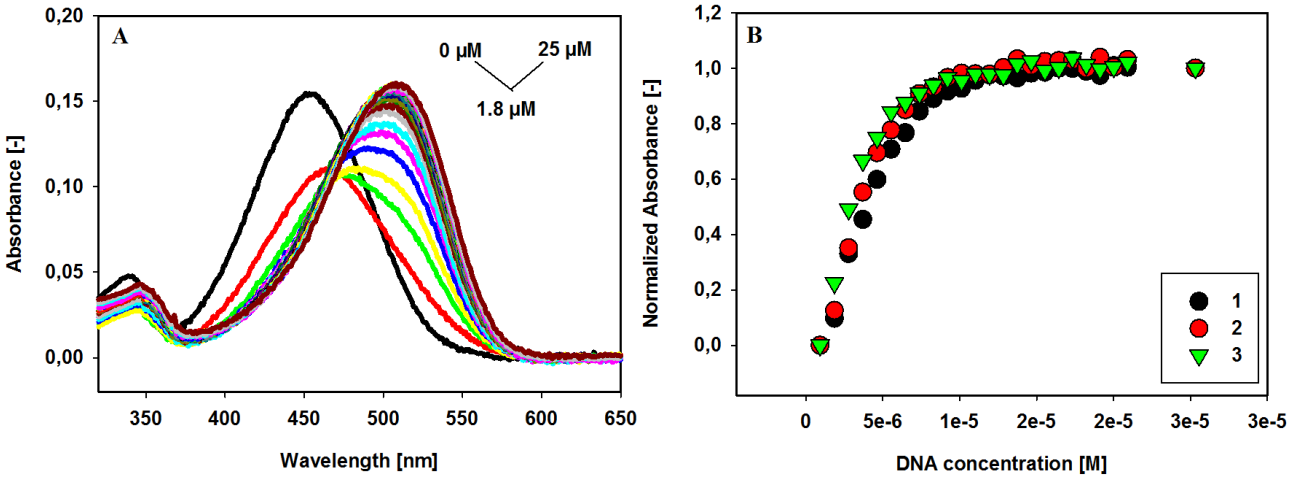

Fig. 3. Spectrophotometric titration of ligand **1** with Pu22 (A) in Tris-HCl buffer (10 mM, pH 7.2) containing 150 mM KCl. Conditions: [L] = 6 µM; titrant: [G4 Pu22] = 713 µM, 10 mM Tris-HCl buffer (pH 7.2), 150 mM KCl. Panel B shows normalized absorbance vs. increasing concentration of Pu22 G-quadruplex at 506 nm (**1**), 508 nm (**2**) and 509 nm (**3**).

3.3. Fluorescence spectroscopy

The binding affinity of carbazole ligands to G-quadruplex c-myc Pu22 was also investigated by fluorescence measurements. The fluorescence spectra recorded at λ_{ex} 506 nm, 508 nm and 509 nm, respectively for ligands **1**, **2,** and **3**, show that the fluorescence of free ligands in a buffer is quite weak. This may be possibly due to the collisional quenching of the excited singlet state by polar water molecules [111]. However, the fluorescence increases significantly in the presence of G-quadruplex c-myc, which may be associated with the hydrophobic environment inside the G-quadruplex that protects ligand from quenching (ligand fluorescence recovery). The intramolecular parallel G-quadruplex in the presence of potassium cations was added to carbazole ligands until very small changes in fluorescence spectra were observed. All three complexes showed enhanced fluorescence in Tris HCl buffer solutions with a maximum wavelength at about 570 nm. At the same time, bathochromic shifts $\Delta\lambda$ = 3 - 5 nm for all ligands were also observed when compared to spectra of complexes (Figs. 4A, S2). Among the ligands tested, compound **3** having an imidazole moiety attached via N-butyl chain to the carbazole, showed the highest fluorescence enhancement (Fig. 4A).

As shown in Fig. 4A, no plateau was observed for titration plots, instead, a gradual rise in saturation plots occurred for all ligands (Fig. S3). Such unusual shape of titration plots may be caused by slow complex dissociation or aggregation processes. In these experiments, ligands **2** and **3** with triazole and imidazole substituents behaved similarly and their fluorescence enhancement (F/Fo) were similar and lower than for ligand **1** with ethyl substituent at the nitrogen atom of carbazole. The lower values of F/Fo may be related to the interaction of azole substituents with the loops and to their ability to form hydrogen bonds. However, relative enhancement in the fluorescence intensities of all ligands is very similar and is correlated with binding constants (Fig. 4C, Table 2).

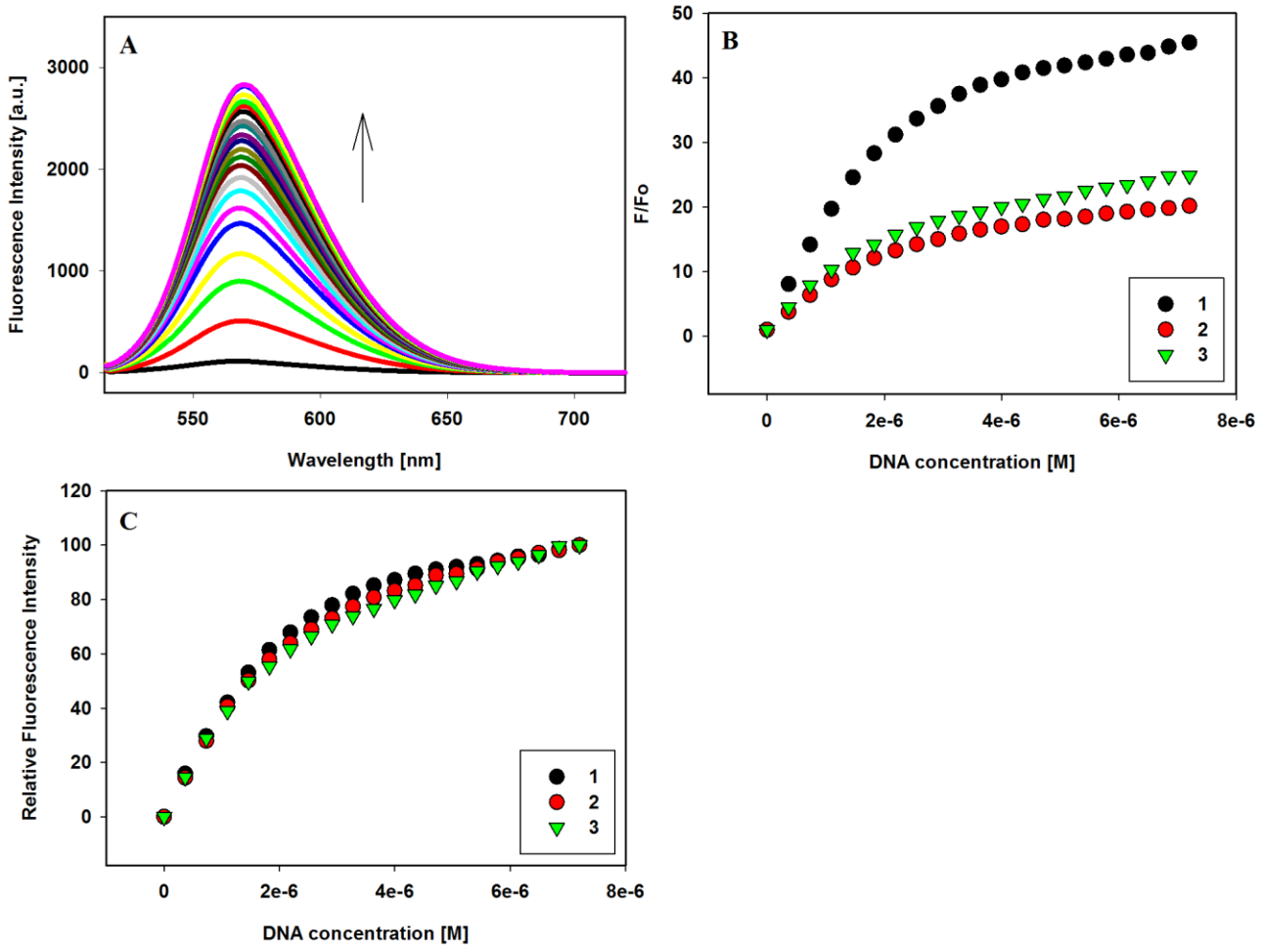

Fig. 4. Fluorescence titration spectra of ligand **3** (2 μM) with G4 Pu22 in Tris-HCl buffer (10 mM,

pH 7.2) containing 150 mM KCl (A); titrant: [G4 Pu22] = 367 μM, 10 mM Tris-HCl buffer (pH 7.2), 150 mM KCl; Fluorescence enhancement curves (B) and relative enhancement in the fluorescence intensities (C) of ligands vs. the increasing concentration of G-quadruplex Pu22; λ_{ex}: **1** - 506 nm, **2** - 508 nm, **3** - 509 nm.

3.4. Binding of ligands to G-Quadruplex Pu22

The UV-VIS and fluorescence titration experiments were used to investigate binding behavior of carbazole ligands **1-3** to c-myc G-quadruplex. The titration plots reached saturations (Fig. 3 B) therefore they were analyzed according to the simple Scatchard model [74,75]. Because of complicated DNA-binding behaviour of ligands **1-3** (blurred isosbestic points, bathochromic shifts, initial hypochromicity followed by hyperchromicity), the estimated binding parameters contain relatively high uncertainty. On the other hand, fluorescence titration plots (Figs. 4, S2) have not reached saturation in the investigated concentration range of G4 DNA, which hampered application of Scatchard model. Instead, we used the Benesi–Hildebrand (B-H) method to estimate binding affinities of investigated ligands [76]. In this case, K_b values can only be estimated with the assumption that stoichiometry of formed ligand/G4 complex is 1:1. Alternatively, result of B-H calculation should be regarded as a nK_b product (Table 2) (Fig. S3).

The intramolecular G-quadruplex Pu22 possesses two potential ligand binding sites, having similar affinities [6]. In the spectrophotometric titration experiments a change in the number of binding sites (n) was decreased and amounted to 0.8, 0.9 and 1.1 (unpublished results). In the fluorescence titration experiments these values were comparable and amounted to 1, 1.1 and 1.1 for ligands **1**,**2** and **3**, respectively. It should be emphasized that in all experiments, G-quadruplex was used in much excess, which implied that the probability to form G4:ligand complexes of 1:1 stoichiometry is higher, than that of 1:2 composition.

Table 2
Parameters for the interaction of ligands **1**, **2** and **3** with Pu22 G-quadruplex determined using Benesi-Hildebrand method in fluorescence titration experiments (K_b - binding constant, n - number of bound ligand molecules per G-quadruplex; **1** - λ_{ex}= 506 nm, **2** - λ_{ex}=508 nm, **3** - λ_{ex}=509 nm).

Ligands	Benesi-Hildebrand method, nK_b ($\times 10^5$ M^{-1})
1	6.9
2	4.0
3	3.9

The spectral properties of the tested ligands permit their use for direct monitoring of binding interactions with oligonucleotides in typical titration experiments with excess of oligonucleotide. Such a titration gives binding data concerning the binding site on oligonucleotide but does not provide information of limiting stoichiometry of oligonucleoide/dye complex. To find out how many carbazole ligands are associated with G4 DNA, we used thiazole orange (TO) as light-up fluorescent probe in G-quadruplex Fluorescent Intercalator Displacement assay (G4-FID) [112,113]. It is known that thiazole orange binds with high affinity to G-quadruplex DNA structures [114] and the binding mode involves the end-stacking interaction of two TO molecules with guanine tetrads [115]. In the absence of DNA, the carbazole ligands **1-3** as well as TO show very low fluorescence quantum yield values in aqueous solutions. Addition of G-quadruplex DNA causes a remarkable enhancement of emission of the dyes because of their binding to G4 structure. The emission spectra recorded at the

excitation wavelength of 480 nm characteristic of TO allow to observe binding equilibria of competing ligands (λ_{em}(TO) = 532 nm and λ_{em}(**3**) = 565 nm). Since stoichiometry of TO/G4 DNA is known, the competition titration of the carbazole ligand/G4 DNA complex with TO will provide spectral changes, which enable determination of stoichiometry for carbazole ligand/G4 complexes. In these experiments, the TO/G4 Pu22 (2:1) complex was titrated with ligand **3** (Fig. 5A) and complex of G4 Pu22 with ligand **3** at the molar ratio of 1:1 (Fig. 5B), and 1:2 (Fig. 5C) were titrated with TO solution. Addition of equimolar concentration of ligand **3** to TO/G4 complex (Fig. 5A) caused disappearence of TO band at 532 nm and evolution of emission at 565 nm in agreement with ligand displacement process and further increase in ligand **3** concentration caused enhancement of emission of G4/ligand **3** complex. Further evidence of 1:2 stoichiometry of G4/ligand **3** complex was provided by FID experiments shown in Figs. 5B and 5C. In the first case (1:1 G4/ligand **3** ratio), TO band appeared just after first titrant addition that indicated association of TO molecule to free tetrad of G4/ligand **3** complex. As expected, an excess of added TO caused disappearance of ligand **3** emission band in accordance with displacement of ligand **3**. Different spectral patterns were observed for titration of G4/ligand **3** solution of 1:2 molar ratio. First two portions of TO did not affect seriously the complex emission band at 565 nm suggesting that binding sites on G4 were already saturated (compare Fig. 5B and Fig. 5C). Increased concentration of TO resulted in broadening of fluorescence band due to the appearance of TO emission at 532 nm. Finally.gradual decrease in emission band is observsd that can be explained by the inner-filter effect or formation of mixed ligand complexes, in which FRET may operate.

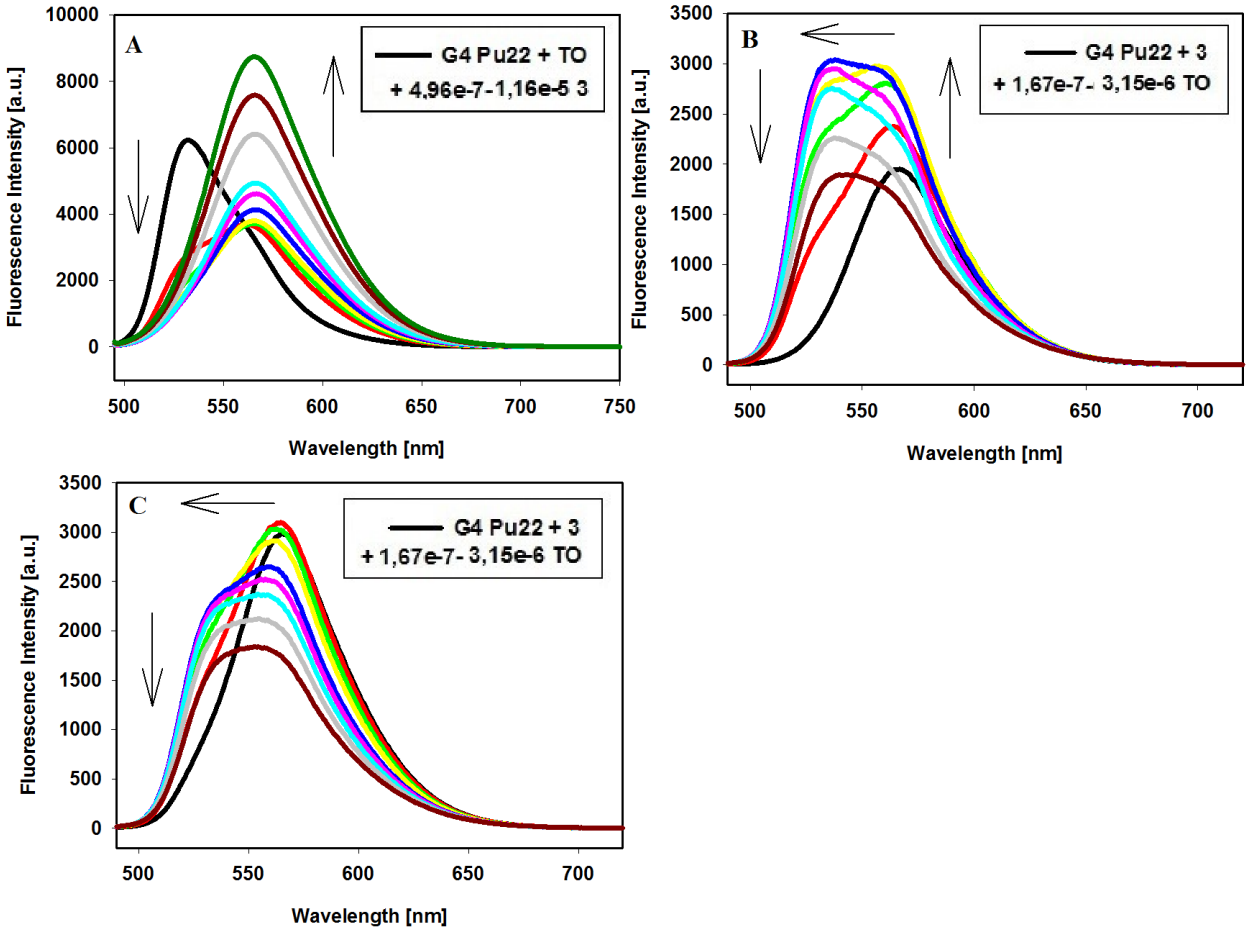

Fig. 5. (A) Fluorescence spectra recorded in FID experiment for ligand **3**; experimental conditions: [G4 Pu22]=0.25 μM, [TO]=0.5 μM, [3] = 0–11.6 μM, 10 mM Tris-HCl buffer (pH 7.2), 150 mM KCl. (B, C) Fluorescence titration experiments of G4/ligand **3** complex with thiazole orange (TO);

experimental conditions: [G4 Pu22]=0.25 μM, [3]= 0.25 μM (B) or 0.5 μM (C), [TO] = 0–3.15 μM, 10 mM Tris-HCl buffer (pH 7.2), 150 mM KCl; λ_{ex} = 480 nm.

The binding stoichiometry of ligands **1-3** to G-quadruplex Pu22 was also determined from fluorescence titration of G4 DNA with ligand. Changes in fluorescence intensity values of the fluorescence bands observed in these experiments are shown in Fig. 6. Upon plotting these values as a function of molar equivalents of carbazole ligands added, one obtains the curves nearly saturated for complexes with all ligands. However, for all three tested complexes the ligand:G4 Pu22 strand ratio is much higher than 1:1, and it is close to binding stoichiometry of 2:1. All our results indicate that the interactions between ligands and G-quadruplex Pu22 are not trivial and may involve formation of a mixture of complexes of the 1:1 and 1:2 stoichiometry, as well as more complex assemblies.

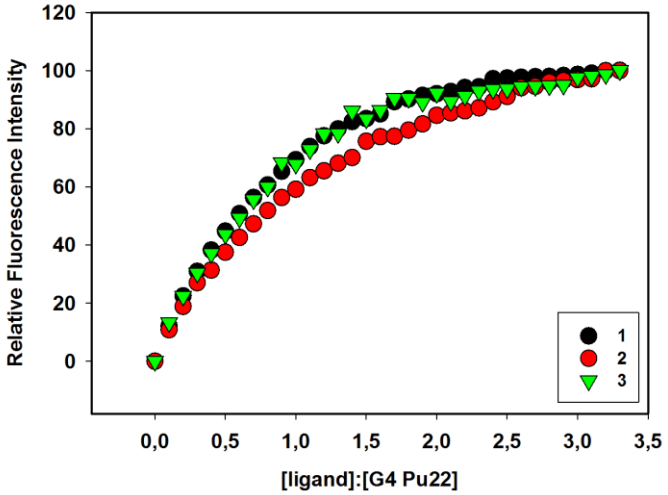

Fig. 6. The increase of normalized fluorescence intensity with added ligands **1-3**.

3.5. CD spectroscopy

Circular dichroism spectroscopy (CD) is a very powerful method for the determination of binding modes of ligands to nucleic acid structures. Circular dichroism was used to investigate the conformational properties of G-quadruplex c-myc Pu22 treated with the carbazole derivatives. Circular dichroism spectra of G4 c-myc Pu22 in Tris HCl buffer were recorded upon addition of carbazole ligands **1-3** (Fig. 7A-C). G4 c-myc Pu22 in 100 mM KCl showed a positive signal at about 265 nm and a negative signal at 241 nm, which suggested a typical parallel G-quadruplex structure [116-118]. The decrease of the both signals in the region of the DNA was observed after addtion of ligands at higher concentration. Because the position of signals have not changed, this may indicate that we don't observe major structural changes of G-quadruplex, but rather the changes in the extent of stacking interaction [119,120]. We do not observe positive induced signals (ICD) in the longwavelength absorption region of carbazole ligands, which rather exclude the groove binding to G-quadruplex structures [121-124]. In all cases, weak negative ICD bands were observed in this region. The CD spectroscopic analysis (Fig. 7A-C) showed that these induced signals were red-shifted above 500 nm. Similar effects were also observed in the UV/Vis titration experiments (Figs. 2A, S1). It should be noted, that the studied ligands have no optical activity, so they do not exhibit CD activity in solution. Thus, the observed CD changes (ICD bands) indicate that the G-quadruplex c-myc Pu22 binds the tested compounds in the same way independently of their substituents and the results suggest similar binding mode for these carbazole ligands.

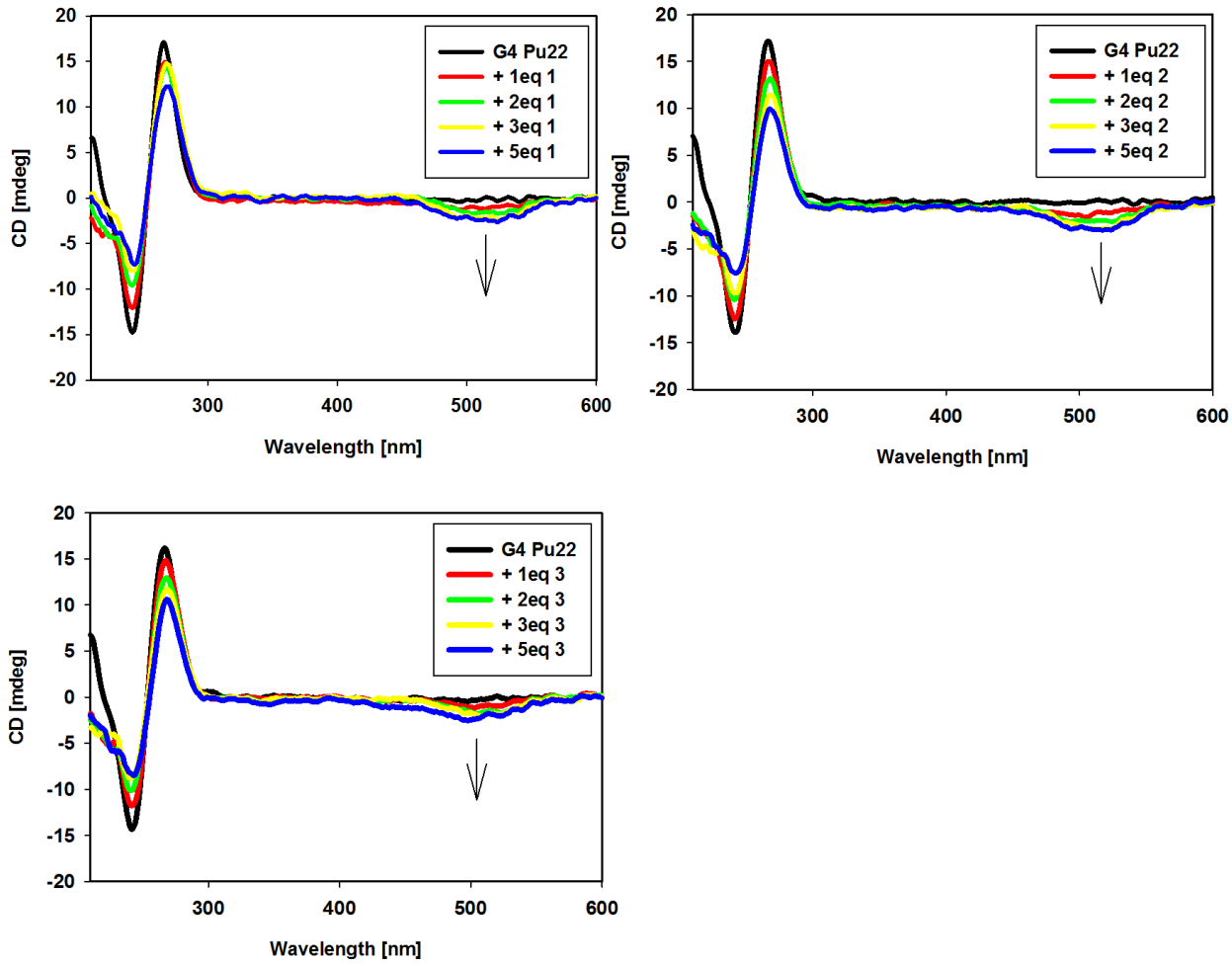

Fig. 7. CD spectra of G-quadruplex Pu22 (5 μM) with increasing concentration of ligands **1** (A), **2** (B) and **3** (C) in Tris-HCl buffer (10 mM, pH 7.2) containing 150mM KCl.

3.6. DNA melting studies.

To determine thermal stabilization of G4 c-myc DNA formed in the presence of each ligand, compared to that of G4 DNA alone, a CD melting study was performed. Initially, G-quadruplex melting experiments were conducted in the presence of 25 mM KCl and 150 mM KCl. Both at high (150 mM) and lower (25 mM) salt concentrations, the quadruplex alone and its complexes were very stable, therefore the precise melting temperatures could not be determined and it was impossible to assess the effect of the ligand binding on stability of the G-quadruplex structure (Table 3). So we have studied the G-quadruplex-complex forming ability through measurements of the thermal melting profiles of the c-myc Pu22 oligonucleotide incubated with carbazole ligands in the absence of K^+. At the wavelength 265 nm, at which there is the characteristic positive CD signal assigned to the oligonucleotide Pu22 and a typical parallel G-quadruplex c-myc structure, significant thermal stabilization was observed after addition of ligands **1-3**. (Fig. 8, Table 3) [60]. Additionally, the melting curves of the oligonucleotide Pu22 showed a hysteresis in the reverse scan, while hysteresis was almost absent in the presence of ligands upon the reverse melting scan.

Table 3
Summary of the DNA melting studies.

Derivative	T_m [°C][a]	ΔT_m [°C][b]	T_m [°C][c]	T_m [°C][d]
No drug	23.4	---	76.8	78.4
1	47.6	24.2	> 80	> 80
2	47.2	23.8	> 80	> 80
3	55.2	31.8	> 80	> 80

[a] T_m of oligonucleotide Pu22 in the absence of salt.
[b] ΔT_m were obtained from the differences in the melting temperatures of the 3 eq ligand bound and oligonucleotide Pu22 in 10 mM Tris-HCl buffer (pH 7.2). Data were collected at 265 nm. Typically three replicate experiments were performed, and average values are reported within ± 1 °C of each other.
[c] T_m values of G4 Pu22 incubated in the presence of 25 mM KCl (lit. 75.5 °C in 20 mM K^+) [5].
[d] T_m values of G4 Pu22 incubated in the presence of 150 mM KCl.

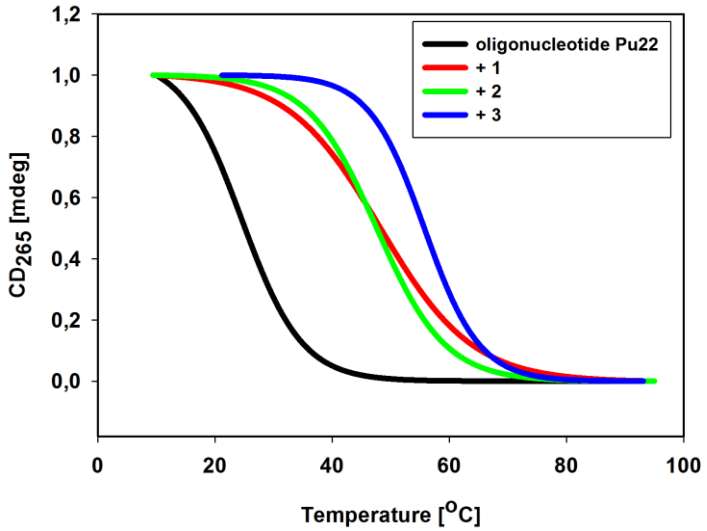

Fig. 8. Normalized CD melting profiles of Pu22 oligonucleotide at 265 nm without and with 3 eq of ligands **1-3** in 10 mM Tris-HCl buffer (pH 7.2).

3.7. Molecular modeling studies.

All ligands (**1-3**) were docked based on template position of indoline structure. Indoline was chosen because it is a common structure, both in quindoline and carbazole. Docking procedures using The Atomic Property Fields (APF) methods in ICM Molsoft program [94] dock ligands based on maximum overlap with the template position. We observe small differences between position of our ligands and template due to difference in the structure and substituents and adaptation to the conformation of the flanking loop residues. We observed that significant binding forces between tetrads and ligands were end-stacking interactions. Triazole and imidazole moieties from ligand **2** and **3** interact at 3' end with T11-A12 loop and at the 5' end with external T1-G2-A3 loop. Both represent almost similar positions after docking procedure. As a result, we obtained ΔG values for each complex after docking to both the 3' end and 5' ends (Fig. 9). Based on those values we selected

the most energetically favourable position of the ligands and G-quadruplex as a starting structure for further simulations.

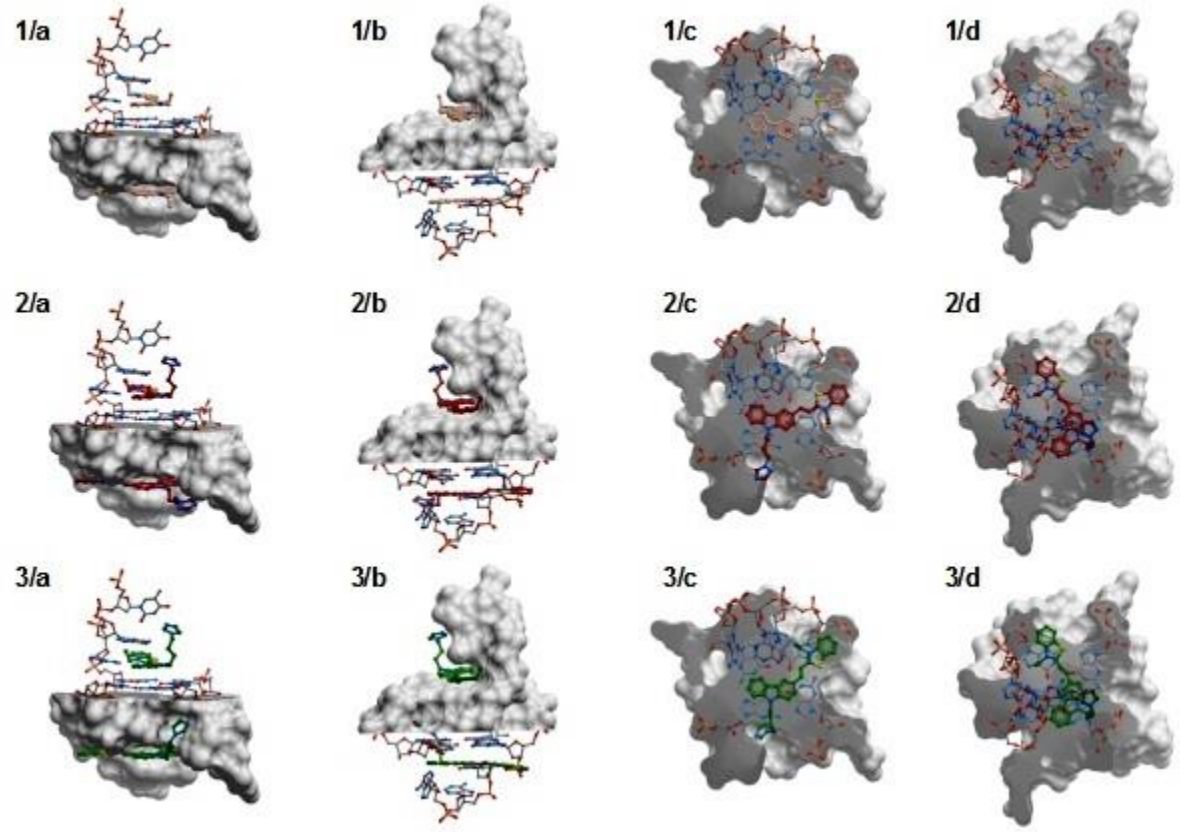

Fig. 9. Docked ligands **1**, **2** and **3** on external G-tetrads of intramolecular parallel-stranded type of G-quadruplex. Cartoons (a) and (b) represents the side view of the complex. In (a), the 5' end is illustrated as sticks and the 3' end in a surface representation. In (b) the 3' end is illustrated as sticks and the 5' end in a surface representation. The next two illustrations highlight the top view of the (c) 5' and (d) 3' ends.

Evaluation of the stability of Pu22/**1,2,3** complexes was assessed based on the interactions and ligand dynamics (Fig. S4). In case of ligand **1** we observe small movement of ligand at the 5' end where carbazole interacted by end-stacking with guanines G6 and G10. We did not observe any interactions with the external T19-A20-A21 and T1-G2-A3 loops. Ligand **2** exhibits good stability at the 5' end. The ligand interacts by end-stacking mode with the tetrad (G4-G7-G13-G17) while triazole moiety is located in the groove making hydrogen bonds (Fig. S5). We did not observe the same behaviour for ligand **2** at the 3'end of G-quadruplex. Ligand **3** translates a lot during simulations due to large freedom of the imidazole moiety with butyl chain linker, which causes destabilization of the two flanking, T19-A20-A21 and T1-G2-A3 loops. Due to this behaviour there were a lot attractive and repulsive interactions between them, which makes both ligand and end loop mobile.

Analysis of the RMSD value (Fig. S6-S7) indicates that our system is indeed well equilibrated but not converged at the current timescale. The results highlight that ligand **2** possesses the best stabilization properties of the three ligands. The structure of G-quaduplex was stable over the course of the simulations. RMSF values (Fig. S8-S9) indicate that two loops T19-A20-A21 and T1-G2-A3 at the ends of the structure are flexible. The triazole moiety interacts with T11-A12 bases and stabilizes that loop, as compared to G4 when no ligand is present. Two significant transition states were observed in case of Pu22/**1** complex. Observed changes were connected with movements

of the external residues T1-G2-A3. The position of the T1 and interaction between them and external G-tetrad (G4-G8-G13-G17) determined observed transition states (Fig. S10). We also observed biggest fluctuations for loop T11-A12 in complex Pu22/**1**. Ligand **1** interacted with tetrads by end-stacking interactions without any movements in the directions of the groove. Also ligand **3** did not create any stable interactions (besides end-stacking), which would enhance the stability of the complex. RMSF value for G-quadruplex DNA without ligands indicate that two loops T19-A20-A21 and T1-G2-A3 were most stable when compared to other complexes. It is connected with the fact that we observe stacking interactions between T1 and external tetrad as well as A21 and external tetrad**.**

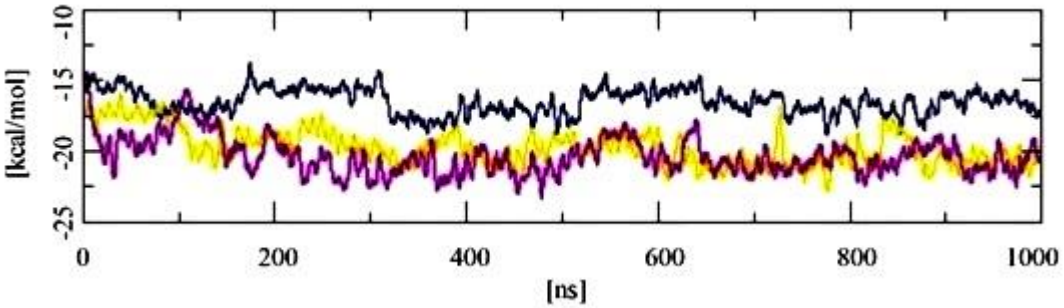

Fig. 10. Binding energy [kcal/mol] computed from the simulations (at 5 frame interval). Blue line represents Pu22/**1** complex, pink line represent Pu22/**2** complex and yellow line represent Pu22/**3** complex.

We computed the value of the binding energy for every 5th frame in the trajectories (Fig. 10) [95]. We observed the lowest value for complexes Pu22/**2** (average value -20.35 [kcal/mol]), for Pu22/**3** (average value -19.77 [kcal/mol]) and Pu22/**1** (average value -16.61 [kcal/mol]). These results are in agreement with the conclusions from clustering analysis, RMSF and RMSD analysis and confirm that ligand **2** better stabilizes the studied G-quadruplex structure. We also observed that after about 200 ns system is equilibrated and the values of binding energy did not change significantly. The obtained results for the complex Pu22/**1** indicate that ligand **1** does not interact with the same affinity with the G-quadruplex. This might be due to interactions just with the tetrad and not with any groove or loops in the G-quadruplex structure.

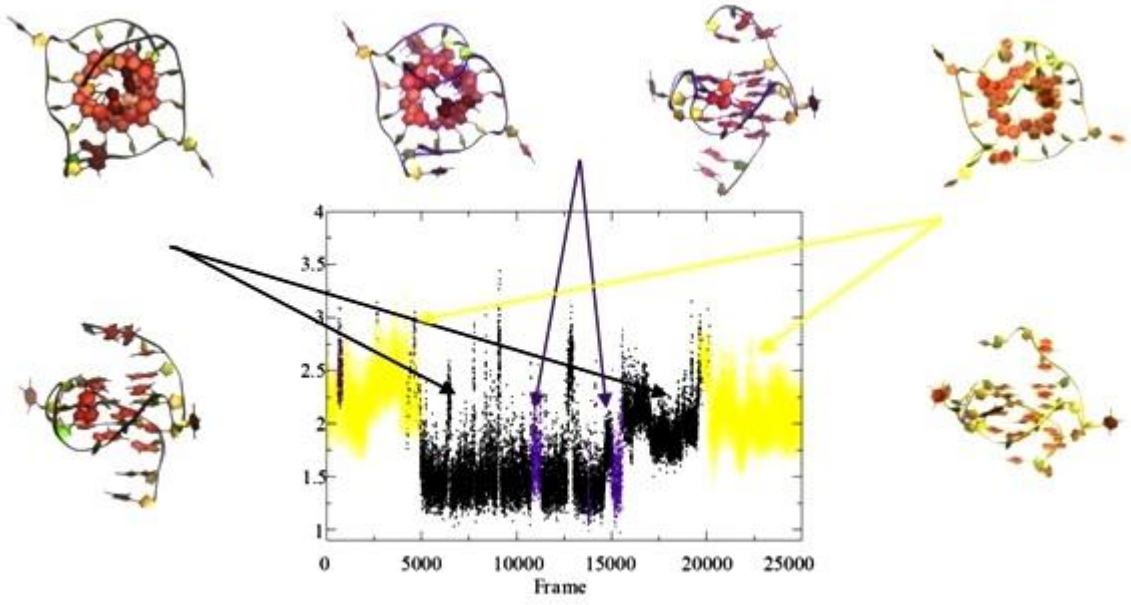

Fig. 11. Conformational clusters obtained by clustering analysis for G-quadruplex-ligand **2** complex. RMSD-based clustering, with a cut-off of 3.75 Å, identified three clusters. Cartoon representations of top (at the 3' end) and side view of cluster centers are illustrated (top 3' end). The violet is a transitional state observed within the black and yellow cluster.

Clustering analysis was conducted for G-quadruplex complex with ligands **1**, **2**, **3** and without any ligand. The aim of clustering analysis is to identify the main substates sampled during the course of the simulation. A 3.75 Å RMSD cut-off identified 5 clusters for DNA conformations simulated without ligand (Fig. S11), 3 clusters for DNA conformations simulated with ligand **1** (Fig. S12 and Fig. S13) and 2 clusters for DNA conformations simulated with ligand **3** (Fig. S14, Fig. S15). In this section we discuss results of G-quadruplex simulated with ligand **2,** while details for ligand **1** and **3** can be found in the supplementary section. A 3.75 Å RMSD cut-off identified three clusters for DNA conformations in complex with **2** (Fig. 11). The top cluster accounted for ~69% of the sampled conformational space. The difference between the obtained clusters and transitional cluster (violet) is connected with conformation of the T1-G2-A3, T19-A20-A21 and T11-A12 loops (Fig. S16). Position of adenine A21 is different in each cluster. Loop T1-G2-A3 is more stable than loop T20-A21-A22 where we observed many changes in the position of all three nucleotides. While we observed alignment of the A3 and G2 nucleotides from the same loop in three centroids on the 5'end loop, we couldn't indicate any such alignment of nucleotides in the 3'end loop. We observe that residues A12 and T11 change conformation when the triazole interacts with the groove. The centroid which represent black cluster corresponds to the G-quadruplex structures conformations that are generated when triazole is not in the groove. The structures observed in the violet cluster are transitional conformations.

4. Conclusions

The main aim of this work was to investigate the interaction of three carbazole ligands, differing in substituent at nitrogen atom of carbazole, with G-quadruplex formed by the DNA sequence derived from the NHE III_1 region of c-myc oncogene (Pu22). The binding of compounds **1**-**3** was investigated by UV-Vis spectrophotometry, fluorescence, CD spectroscopy, and molecular modeling. The results have shown that all ligands have ability to stabilize the intramolecular G-quadruplex Pu22 and interact by the same binding mode. The spectrophotometric titration results have shown a trend towards large hypochromicity at lower G4/ligand ratios followed by hyperchromic effect at higher G4 concentrations, which indicates the presence of more than one binding mode.Being weakly fluorescent in aqueous solution, these vinylic derivatives of carbazole display strong fluorescence enhancement when bound to c-myc G-quadruplex. CD melting studies indicate that the ligands have the ability to form and stabilize the c-myc G-quadruplex structure. The experimental results indicate that the ligand **1** shows the strongest interactions with the tested c-myc G-quadruplex, however, the strength of interaction with ligand **2** is almost at the same level. This is consistent with the results of molecular modeling, where ligand **2** possessed the best stabilization properties of G-quadruplex. However, the simple correlation between energy values and complex stability was not observed, which indicates that strong interactions between ligand and G-quadruplex do not necessarily result in better stability of the system. Altogether, the data indicate that carbazole skeleton is an attractive scaffold for further structural modifications.

Acknowledgment

This research was cofinancially supported by the Foundation for Polish Science within the PARENT-BRIDGE programme (grant number POMOST-2011-3/3). SH is a UCL Career Excellence Fellow.

References

[1] G.N. Parkinson, M.P.H. Lee, S. Neidle, Crystal structure of parallel quadruplexes from human telomeric DNA, Nature 417 (2002) 876-880.
[2] A. Siddiqui-Jain, C.L. Grand, D.J. Bearss, L.H. Hurley, Direct evidence for a G-quadruplex in a promoter region and its targeting with a small molecule to repress c-MYC transcription, Proc. Nat. Acad. Sci. U. S. A. 99 (2002) 11593-11598.
[3] H.J. Lipps, D. Rhodes, G-quadruplex structures: *in vivo* evidence and function, Trends Cell Biol. 19 (2009) 414-422.
[4] G. Biffi, D. Tannahill, J. McCafferty, S. Balasubramanian, Quantitative visualization of DNA G-quadruplex structures in human cells, Nature Chemistry 5 (2013) 182-186.
[5] R.I. Mathad, E. Hatzakis, J. Dai, D. Yang, c-MYC promoter G-quadruplex formed at the 5'-end of NHE III1 element: insights into biological relevance and parallel-stranded G-quadruplex stability, Nucleic Acids Res. 39 (2011) 9023-9033.
[6] J. Dai, M. Carver, L.H. Hurley, D. Yang, Solution structure of a 2:1 quindoline-c-MYC G-quadruplex: insights into G-quadruplex-interactive small molecule drug design, J. Am. Chem. Soc. 133 (2011) 17673-17680.
[7] T. Simonsson, P. Pecinka, M. Kubista, DNA tetraplex formation in the control region of c-myc, Nucleic Acids Res. 26 (1998) 1167-1172.
[8] S. Rankin, A.P. Reszka, J. Huppert, M. Zloh, G.N. Parkinson, A.K. Todd, S. Ladame, S. Balasubramanian, S. Neidle, Putative DNA quadruplex formation within the human c-kit oncogene, J. Am. Chem. Soc. 127 (2005) 10584-10589.
[9] H. Fernando, A.P. Reszka, J. Huppert, S. Ladame, S. Rankin, A.R. Venkitaraman, S. Neidle, S. Balasubramanian, A conserved quadruplex motif located in a transcription activation site of the human c-kit oncogene, Biochemistry 45 (2006) 7854-7860.
[10] T.S. Dexheimer, D. Sun, L.H. Hurley, Deconvoluting the structural and drug-recognition complexity of the G-quadruplex-forming region upstream of the bcl-2 P1 promoter, J. Am. Chem. Soc. 128 (2006) 5404-5415.
[11] P. Agrawal, C. Lin, R.I. Mathad, M. Carver, D. Yang, The Major G-Quadruplex Formed in the Human BCL-2 Proximal Promoter Adopts a Parallel Structure with a 13-nt Loop in K^+ Solution, J. Am. Chem. Soc. 136 (2014) 1750-1753.
[12] K. Guo, A. Pourpak, K. Beetz-Rogers, V. Gokhale, D. Sun, L.H. Hurley, Formation of pseudosymmetrical G-quadruplex and i-motif structures in the proximal promoter region of the RET oncogene, J. Am. Chem. Soc. 129 (2007) 10220-10228.
[13] X. Tong, W. Lan, X. Zhang, H. Wu, M. Liu, C. Cao, Solution structure of all parallel G-quadruplex formed by the oncogene *RET* promoter sequence, Nucleic Acids Res. 39 (2011) 6753-6763.
[14] A. Ambrus, D. Chen, J. Dai, R.A. Jones, D. Yang, Solution structure of the biologically relevant G-quadruplex element in the human c-MYC promoter. Implications for G-quadruplex stabilization, Biochemistry 44 (2005) 2048-2058.
[15] A.T. Phan, V.V. Kuryavyi, S. Burge, S. Neidle, D.J. Patel, Structure of an Unprecedented G-Quadruplex Scaffold in the Human c-kit Promoter, J. Am. Chem. Soc. 129 (2007) 4386-4392.
[16] S.-T.D. Hsu, P. Varnai, A. Bugaut, A.P. Reszka, S. Neidle, S. Balasubramanian, A G-Rich Sequence within the *c-kit* Oncogene Promoter Forms a Parallel G-Quadruplex Having Asymmetric G-Tetrad Dynamics, J. Am. Chem. Soc. 131 (2009) 13399-13409.

[17] V. Kuryavyi, A.T. Phan, D.J. Patel, Solution structures of all parallel-stranded monomeric and dimeric G-quadruplex scaffolds of the human *c-kit2* promoter, *Nucleic Acids Res.* 38 (2010) 6757-6773.
[18] D. Wei, G.N. Parkinson, A.P. Reszka, S. Neidle, Crystal structure of a *c-kit* promoter quadruplex reveals the structural role of metal ions and water molecules in maintaining loop conformation, Nucleic Acids Res. 40 (2012) 4691-4700.
[19] J. Dai, D. Chen, R.A. Jones, L.H. Hurley, D. Yang, NMR solution structure of the major G-quadruplex structure formed in the human BCL2 promoter region, Nucleic Acids Res. 34 (2006) 5133-5144.
[20] D. Sen, W. Gilbert, Formation of parallel four-stranded complexes by guanine-rich motifs in DNA and its implications for meiosis, Nature 334 (1988) 364-366.
[21] T. Simonsson, G-Quadruplex DNA Structures Variations on a Theme, Biol. Chem. 382 (2001) 621-628.
[22] S. Neidle, S. Balasubramanian, Quadruplex Nucleic Acids, RSC, Cambrige, 2006.
[23] T. Ou, Y. Lu, J. Tan, Z. Huang, K. Wong, L. Gu, G-Quadruplexes: Targets in Anticancer Drug Design, ChemMedChem 3 (2008) 690-713.
[24] A. De Cian, L. Lacroix, C. Douarre, N. Temime-Smaali, C. Trentesaux, J.-F. Riou, J.-L. Mergny, Targeting telomeres and telomerase, Biochemie 90 (2008) 131-155.
[25] C.A. Spencer, M. Groudine, Control of c-*myc* Regulation in Normal and Neoplastic Cells, Adv. Cancer Res. 56 (1991) 1-48.
[26] S. Pelengaris, B. Rudolph, T. Littlewood, Action of Myc *in vivo* — proliferation and apoptosis, Curr. Opin. Genet. Dev. 10 (2000) 100-105.
[27] W. Lutz, J. Leon, M. Eilers, Contributions of Myc to tumorigenesis, Biochim. Biophys. Acta, Rev. Cancer 1602 (2002) 61-71.
[28] M. Eilers, R.N. Eisenman, Myc's broad reach, Genes Dev. 22 (2008) 2755-2766.
[29] N. Meyer, L.Z. Penn, Reflecting on 25 years with MYC, Nat. Rev. Cancer 8 (2008) 976-990.
[30] E.H. Postel, S.E. Mango, S.J. Flint, A nuclease-hypersensitive element of the human c-myc promoter interacts with a transcription initiation factor, Mol. Cell. Biol. 9 (1989) 5123-5133.
[31] T.L. Davis, A.B. Firulli, A.J. Kinniburgh, Ribonucleoprotein and protein factors bind to an H-DNA-forming c-myc DNA element: possible regulators of the c-myc gene, Proc. Natl. Acad. Sci. U. S. A. 86 (1989) 9682-9686.
[32] S.J. Berberich, E.H. Postel, PuF/NM23-H2/NDPK-B transactivates a human c-myc promoter-CAT gene via a functional nuclease hypersensitive element, Onkogene, 10 (1995) 2343-2347.
[33] J.-F. Riou, G-Quadruplex Interacting Agents Targeting the Telomeric G-Overhang Are More than Simple Telomerase Inhibitors, Curr. Med. Chem. Anti-Cancer Agents 4 (2004) 439-443.
[34] L.R. Kelland, Overcoming the immortality of tumour cells by telomere and telomerase based cancer therapeutics – current status and future prospects, Eur. J. Cancer 41 (2005) 971-979.
[35] M. Folini, P. Gandellini, N. Zaffaroni, Targeting the telosome: Therapeutic implications, Biochim. Biophys. Acta 1792 (2009) 309-316.
[36] T.A. Brooks, L.H. Hurley, Targeting MYC Expression through G-Quadruplexes, Genes Cancer 1 (2010) 641-649.
[37] D.Z. Yang, K. Okamoto, Structural insights into G-quadruplexes: towards new anticancer drugs, Future Med. Chem. 2 (2010) 619-646.
[38] J. Bidzinska, G. Cimino-Reale, N. Zaffaroni, M. Folino, G-Quadruplex Structures in the Human Genome as Novel Therapeutic Targets, Molecules 18 (2013) 12368-12395.
[39] S.A. Ohnmacht, S. Neidle, Small-molecule quadruplex-targeted drug discovery, Bioorg. Med. Chem. Lett. 24 (2014) 2602-2612.
[40] V. Sekaran, J. Soares, M.B. Jarstfer, Telomere Maintenance as a Target for Drug Discovery, J. Med. Chem. 57 (2014) 521-538.

[41] G.W. Collie, R. Promontorio, S.M. Hampel, M. Micco, S. Neidle, G.N. Parkinson, Structural Basis for Telomeric G-Quadruplex Targeting by Naphthalene Diimide Ligands, *J. Am. Chem. Soc.* 134 (2012) 2723–2731.
[42] R. Haudecoeur, L. Stefan, F. Denat, D. Monchaud, A Model of Smart G-Quadruplex Ligand, J. Am. Chem. Soc. 135 (2013) 550-553.
[43] Md.M. Islam, S. Fujii, S. Sato, T. Okauchi, S. Takenaka, A Selective G-Quadruplex DNA-Stabilizing Ligand Based on a Cyclic Naphthalene Diimide Derivative, *Molecules* 20 (2015) 10963-10979.
[44] Y.-H. Lin, S.-M. Chuang, P.-C. Wu, C.-L. Chen, S. Jeyachandran, S.-C. Lo, H.-S. Huang, M.-H. Hou, Selective recognition and stabilization of new ligands targeting the potassium form of the human telomeric G-quadruplex DNA, Scientific Rep. 6 (2016) 31019.
[45] E. Rajczak, A. Gluszynska, B. Juskowiak, Interaction of metallacrown complexes with G-quadruplex DNA, J. Inorg. Biochem. 155 (2016) 105–114.
[46] E. Rajczak, V.L. Pecoraro, B. Juskowiak, Sm(III)[12-MCGa(III)shi-4] as a luminescent probe for G-quadruplex structures, *Metallomics*, 9 (2017) 1735-1744.
[47] H. Qin, C. Zhao, Y. Sun, J. Ren, X. Qu, Metallo-supramolecular complexes enantioselectively eradicate cancer stem cells in vivo *J. Am. Chem. Soc.* 139 (2017) 16201–16209.[48] T.V.T. Le, S. [48] Han, J. Chae, H.J. Park, G-Quadruplex Binding Ligands: from Naturally Occurring to Rationally Designed Molecules, Curr. Pharm. Des. 18 (2012) 1948-1972.
[49] C.L. Grand, H. Han, R.M. Munoz, S. Weitman, D.D. Von Hoff, L.H. Hurley, D.J. Bearss, The cationic porphyrin TMPyP4 down-regulates c-MYC and human telomerase reverse transcriptase expression and inhibits tumor growth *in vivo*, Mol. Cancer Ther. 1 (2002) 565-573.
[50] J. Seenisamy, S. Bashyam, V. Gokhale, H. Vankayalapati, D. Sun, A. Siddiqui-Jain, N. Streiner, K. Shinya, E. White, W.D. Wilson, L.H. Hurley, Design and Synthesis of an Expanded Porphyrin That Has Selectivity for the c-MYC G-Quadruplex Structure, J. Am. Chem. Soc. 127 (2005) 2944-2959.
[51] A.T. Phan, V. Kuryavyi, H.Y. Gaw, D. Patel, Small-molecule interaction with a five-guanine-tract G-quadruplex structure from the human MYC promoter, Nat. Chem. Biol. 1 (2005) 167-173.
[52] V. Gabelica, E.S. Baker, M.-P. Teulade-Fichou, E. De Pauw, M.T. Bowers, Stabilization and Structure of Telomeric and c-myc Region Intramolecular G-Quadruplexes: The Role of Central Cations and Small Planar Ligands, J. Am. Chem. Soc. 129 (2007) 895-904.
[53] M. Petenzi, D. Verga, E. Largy, F. Hamon, F. Doria, M.-P. Teulade-Fichou, A. Guédin, J.-L. Mergny, M. Mella, M. Freccero, Cationic Pentaheteroaryls as Selective G-Quadruplex Ligands by Solvent-Free Microwave-Assisted Synthesis, Chem. Eur. J. 18 (2012) 14487-14496.
[54] D. Drygin, A. Siddiqui-Jain, S. O'Brien, M. Schwaebe, A. Lin, J. Bliesath, C.B. Ho, C. Proffitt, K. Trent, J.P. Whitten, J.K.C. Lim, D. Von Hoff, K. Anderes, W.G. Rice, Anticancer Activity of CX-3543: A Direct Inhibitor of rRNA Biogenesis, Cancer Res. 69 (2009) 7653-7661.
[55] D.S.-H. Chan, H. Yang, M.H.-T. Kwan, Z. Cheng, P. Lee, L.-P. Bai, Z.-H. Jiang, C.-Y. Wong, W.-F. Fong, C.-H. Leung, D.-L. Ma, Structure-based optimization of FDA-approved drug methylene blue as a c-myc G-quadruplex DNA stabilizer, Biochimie 93 (2011) 1055-1064.
[56] H.-M. Lee, D.S.-H. Chan, F. Yang, H.-Y. Lam, S.-C. Yan, C.-M. Che, D.-L. Ma, C.-H. Leung, Identification of natural product Fonsecin B as a stabilizing ligand of c-*myc* G-quadruplex DNA by high-throughput virtual screening, Chem. Comm. 46 (2010) 4680-4682.
[57] Y. Ma, T.-M. Ou, J.-H. Tan, J.-Q. Hou, S.-L. Huang, L.-Q. Gu, Z.-S. Huang, Quinolino-benzo-[5, 6]-dihydroisoquindolium compounds derived from berberine: A new class of highly selective ligands for G-quadruplex DNA in *c-myc* oncogene, Eur. J. Med. Chem. 46 (2011) 1906-1913.
[58] W.-J. Chen, C.-X. Zhou, P.-F. Yao, X.-X. Wang, J.-H. Tan, D. Li, T.-M. Ou, L.-Q. Gu, Z.-S. Huang, Disubstituted 1,8-dipyrazolcarbazole derivatives as a new type of *c-myc* G-quadruplex binding ligands, Bioorg. Med. Chem. 20 (2012) 2829-2836.

[59] B. Dumat, G. Bordeau, E. Faurel-Paul, F. Mahuteau-Betzer, N. Saettel, M. Bombled, G. Metgé, F. Charra, C. Fiorini-Debuisschert, M.-P. Teulade-Fichou, *N*-phenyl-carbazole-based two-photon fluorescent probes: Strong sequence dependence of the duplex *vs* quadruplex selectivity, Biochimie 93 (2011) 1209-1218.
[60] T.-M. Ou, Y.-J Lu., C. Zhang, Z.-S. Huang, X.-D. Wang, J.-H. Tan, Y. Chen, D.-L. Ma, K.-Y. Wong, J.C.-O. Tang, A.S.-C. Chan, L.-Q. Gu, Stabilization of G-Quadruplex DNA and Down-Regulation of Oncogene *c-myc* by Quindoline Derivatives, J. Med. Chem. 50 (2007) 1465-1474.
[61] P. Wu, D.-L. Ma, C.-H. Leung, S.-C. Yan, N. Zhu, R. Abagyan, C.-M. Che, Stabilization of G-Quadruplex DNA with Platinum(II) Schiff Base Complexes: Luminescent Probe and Down-Regulation of c-*myc* Oncogene Expression, Chem. Eur. J. 15 (2009) 13008-13021.
[62] P. Wang, C.-H. Leung, D.-L. Ma, S.-C. Yan, C.-M. Che, Structure-based design of platinum(II) complexes as c-myc oncogene down-regulators and luminescent probes for G-quadruplex DNA, Chem. Eur. J. 16 (2010) 6900-6911.
[63] Z.-F. Chen, Q.-P. Qin, J.-L. Qin, Y.-C. Liu, K.-B. Huang, Y.-L. Li, T. Meng, G.-H. Zhang, Y. Peng, X.-J. Luo, H. Liang, Stabilization of G-Quadruplex DNA, Inhibition of Telomerase Activity, and Tumor Cell Apoptosis by Organoplatinum(II) Complexes with Oxoisoaporphine, J. Med. Chem. 58 (2015) 2159-2179.
[64] C. Wei, L. Ren, N. Gao, Interactions of terpyridines and their Pt(II) complexes with G-quadruplex DNAs and telomerase inhibition, Int. J. Biol. Macromol. 57 (2013) 1-8.
[65] Q.-P. Qin, J.-L. Qin, T. Meng, W.-H. Lin, C.-H. Zhang, Z.-Z. Wei, J.-N. Chen, Y.-C. Liu, H. Liang, Z.-F. Chen, High in vivo antitumor activity of cobalt oxoisoaporphine complexes by targeting G-quadruplex DNA, telomerase and disrupting mitochondrial functions, Eur. J. Med. Chem. 124 (2016) 380-392.
[66] C.W. Ong, M.-C. Liu, K.-D. Lee, K.W. Chang, Y.-T. Yang, H.-W. Tung, K.R. Fox, Synthesis of bisquinoline-pyrrole oligoamide as G-quadruplex binding ligand, Tetrahedron 68 (2012) 5453-5457.
[67] K.V. Diveshkumar, S. Sakrikar, F. Rosu, S. Harikrishna, V. Gabelica, P.I. Pradeepkumar, Specific Stabilization of c-MYC and c-KIT G-Quadruplex DNA Structures by Indolylmethyleneindanone Scaffolds, Biochemistry 55 (2016) 3571-3585.
[68] J. Alzeer, N.W. Luedtke, pH-Mediated Fluorescence and G-Quadruplex Binding of Amido Phthalocyanines, Biochemistry 49 (2010) 4339-4348.
[69] V. Dhamodharan, S. Harikrishna, A.C. Bhasikuttan, P.I. Pradeepkumar, Topology Specific Stabilization of Promoter over Telomeric G-Quadruplex DNAs by Bisbenzimidazole Carboxamide Derivatives, ACS Chem. Biol. 10 (2015) 821-833.
[70] E. Micheli, A. Altieri, L. Cianni, C. Cingolani, S. Iachettini, A. Bianco, C. Leonetti, S. Cacchione, A. Biroccio, M. Franceschin, A. Rizzo, Perylene and coronene derivatives binding to G-rich promoter oncogene sequences efficiently reduce their expression in cancer cells, Biochimie 125 (2016) 223-231.
[71] A.W. Schmidt, K.R. Reddy, H.-J. Knölker, Occurrence, Biogenesis, and Synthesis of Biologically Active Carbazole Alkaloids, Chem. Rev. 112 (2012) 3193-3328.
[72] A. Głuszyńska, Biological potential of carbazole derivatives, Eur. J. Med. Chem. 94 (2015) 405-426.
[73] L. Zhang, X.-M. Peng, G.L.V. Damu, R.-X. Geng, C.-H. Zhou, Comprehensive review in current developments of imidazole-based medicinal chemistry, Med. Res. Rev. 34 (2014) 340-437.
[74] C.H. Zhou, Y. Wang, Curr. Recent researches in triazole compounds as medicinal drugs, Med. Chem. 19 (2012) 239-280.
[75] R. Kaur, A.R. Dwivedi, B. Kumar, V. Kumar, Recent Developments on 1,2,4-Triazole Nucleus in Anticancer Compounds: A Review, Anticancer Agents Med. Chem. 16 (2016) 465-489.

[76] C. Saengkhae, M. Salerno, D. Adès, A. Siove, L. Le Moyec, V. Migonney, A. Garnier-Suillerot, Ability of carbazole salts, inhibitors of Alzheimer β-amyloid fibril formation, to cross cellular membranes, Eur. J. Pharmacology 559 (2007) 124-131.
[77] unpublished results.
[78] A. Głuszyńska, E. Rajczak, B. Juskowiak, Synthesis and spectroscopic characterisation of (*E*)-2-(2-(9-(4-(1*H*-1,2,4-triazol-1-yl)butyl)-9*H*-carbazol-3-yl)vinyl)-3-ethylbenzo[*d*]thiazol-3-ium, a new ligand and potential DNA intercalator, Chemical Papers 67 (2013) 1231-1239.
[79] A.V. Tataurov, Y. You, R. Owczarzy, Predicting ultraviolet spectrum of single stranded and double stranded deoxyribonucleic acids, Biophys. Chem. 133 (2008) 66-70.
[80] G. Scatchard, The attraction of proteins for small molecules and ions, Ann. N. Y. Acad. Sci. 51 (1949) 660-672.
[81] J.B. Chairs, Analysis and interpretation of ligand-DNA binding isotherms, Methods Enzymol. 340 (2001) 3-22.
[82] G.A. Crosby, J.N. Demas, Measurement of photoluminescence quantum yields. Review, J. Phys. Chem. 75 (1971) 991-1024.
[83] J. Wang, R.M., Wolf J.W. Caldwell, P.A. Kollman, D.A. Case, Development and testing of a general amber force field, J. Comput. Chem. 25 (2004) 1157-1174.
[84] V. Hornak, R. Abel, A. Okur, B. Strockbine, A. Roitberg, C. Simmerling, Comparison of multiple Amber force fields and development of improved protein backbone parameters, Proteins 65 (2006) 712-725.
[85] A. Pérez, I. Marchán, D. Svozil, J. Sponer, T.E. Cheatham, C.A. Laughton, M. Orozco, Refinement of the AMBER Force Field for Nucleic Acids: Improving the Description of α/γ Conformers, Biophys. J. 92 (2007) 3817-3829.
[86] M. Zgarbová, M. Otyepka, J. Šponer, A. Mládek, P. Banáš, T.E. Cheatham, P. Jurečka, Refinement of the Cornell et al. Nucleic Acids Force Field Based on Reference Quantum Chemical Calculations of Glycosidic Torsion Profiles, J. Chem. Theory Comput. 7 (2011) 2886-2902.
[87] P. Banáš, D. Hollas, M. Zgarbová, P. Jurečka, M. Orozco, T.E. Cheatham, J. Šponer, M. Otyepka, Performance of Molecular Mechanics Force Fields for RNA Simulations: Stability of UUCG and GNRA Hairpins, J. Chem. Theory Comput. 6 (2010) 3836-3849.
[88] D.A. Case, T.E. Cheatham, T. Darden, H. Gohlke, R. Luo, K.M. Merz, A. Onufriev, C. Simmerling, B. Wang, R.J. Woods, The Amber biomolecular simulation programs, J. Comput. Chem. 26 (2005) 1668-1688.
[89] M. Totrov, Atomic Property Fields: Generalized 3D Pharmacophoric Potential for Automated Ligand Superposition, Pharmacophore Elucidation and 3D QSAR, Chem. Biol. Drug Des. 71 (2008) 15-27.
[90] J. Wang, R.M. Wolf, J.W. Caldwell, P.A. Kollman, D.A. Case, Development and testing of a general amber force field, J. Comput. Chem. 25 (2004) 1157-1174.
[91] M.J. Harvey, G. Giupponi, G.D. Fabritiis, ACEMD: Accelerating Biomolecular Dynamics in the Microsecond Time Scale, J. Chem. Theory Comput. 5 (2009) 1632-1639.
[92] D. Van Der Spoel, E. Lindahl, B. Hess, G. Groenhof, A.E. Mark, H.J.C. Berendsen, GROMACS: Fast, flexible, and free, J. Comput. Chem. 26 (2005) 1701-1718.
[93] W. Humphrey, A. Dalke, K. Schulten, VMD: Visual molecular dynamics, J. Molec. Graphics, 14 (1996) 33-38.
[94] R.A. Abagyan, M.M. Totrov, D.N. Kuznetsov, ICM—A new method for protein modeling and design: Applications to docking and structure prediction from the distorted native conformation, J. Comp. Chem. 15 (1994) 488-506.
[95] O. Trott, A.J. Olson, AutoDock Vina: Improving the Speed and Accuracy of Docking with a New Scoring Function, Efficient Optimization, and Multithreading, J. Comput. Chem. 31 (2010) 455-461.

[96] R. Wang, L. Lai, S. Wang, Further development and validation of empirical scoring functions for structure-based binding affinity prediction, J. Comput. Aided Mol. Des. 16 (2002) 11-26.
[97] A. Głuszyńska, E. Rajczak, J. Kosman, B. Juskowiak, Interactions of new carbazole ligands, potential inhibitors of telomerase, with different structures of DNA: A comparative study, Proceedings of the 40th International Conference of Slovak Society of Chemical Engineering, Tatranské Matliare, Slovakia (2013) 1326-1332.
[98] A. Głuszyńska, E. Rajczak, M. Gołdys, B. Juskowiak, The interaction of n-ethyl carbazole ligand with the guanine-rich dna strand in the kras onkogene promoter, Proceedings of the 43th International Conference of Slovak Society of Chemical Engineering, Tatranské Matliare, Slovakia (2016) 827-832.
[99] M. Boiani, M. Gonzalez, Imidazole and Benzimidazole Derivatives as Chemotherapeutic Agents, Mini Rev. Med. Chem. 5 (2005) 409-424.
[100] L. De Luca, Naturally occurring and synthetic imidazoles: their chemistry and their biological activities, Curr Med Chem. 13 (2006) 1-23.
[101] D. Hernández Romero, V.E. Torres Heredia, O. García-Barradas, Ma. E. Márquez López, E. Sánchez Pavón, Synthesis of imidazole derivatives and their biological activities, J. Chem. Biochem., 2 (2014) 45-83.
[102] Y. Wang, C.H. Zhou, Recent advances in the researches of triazole compounds as medicinal drugs, Sci. Sinca Chim. 41 (2011) 1429-1456.
[103] J. Sharma, S. Ahmad, M.S. Alam, A Shamsher, Bioactive Triazoles: A potential review, J. Chem. Pharm. Res. 4 (2012) 5157-5164.
[104] M. Asif, Biological Potentials of Biological Active Triazole Derivatives: A Short Review, Org. Chem. Curr. Res. 5 (2016) 8 pages.
[105]. F.-F. Zhang, L.-L. Gan, C.-H. Zhou, Synthesis, antibacterial and antifungal activities of some carbazole derivatives, Bioorg. Med. Chem. Lett. 20 (2010) 1881-1884.
[106] R.F. Pasternack, E.J. Gibbs, J.J. Villaffranca, Interactions of porphyrins with nucleic acids, Biochemistry 22 (1983) 2406-2414.
[107] M.W. Freyer, R. Buscaglia, K. Kaplan, D. Cashman, L.H. Hurley, E.A. Lewis, Biophysical Studies of the c-MYC NHE III1 Promoter: Model Quadruplex Interactions with a Cationic Porphyrin, Biophys. J. 92 (2007) 2007-2015.
[108] A. Slama-Schwok, M. Rougee, V. Ibanez, N. E. Geacintov, T. Montenay-Garestier, J.M. Lehn, C. Hélène, Interactions of the dimethyldiazaperopyrenium dication with nucleic acids. 2. Binding to double-stranded polynucleotides, Biochemistry 28 (1989) 3234-3242.
[109] Y. Wang, A. Zhou, Spectroscopic studies on the binding of methylene blue with DNA by means of cyclodextrin supramolecular systems, J. Photochem. Photobiol. A Chem. 190 (2007) 121–127.
[110] D. Shiu-Hin Chan, H. Yang, M. Hiu-Tung Kwan, Z. Cheng, P. Lee, L.-P. Bai, Z.-H. Jiang, C.-Y. Wong, W.-F. Fong, C.-H. Leung, D.-L. Ma, Structure-based optimization of FDA-approved drug methylene blue as a c-myc G-quadruplex DNA stabilizer, Biochimie 93 (2011) 1055-1064.
[111] B. Maji, K. Kumar, K. Muniyappa, S. Bhattacharya, New dimeric carbazole–benzimidazole mixed ligands for the stabilization of human telomeric G-quadruplex DNA and as telomerase inhibitors. A remarkable influence of the spacer, Org. Biomol. Chem. 13 (2015) 8335-8348.
[112] D. Monchaud, C. Allain, M.-P. Teulade-Fichou, Development of a fluorescent intercalator displacement assay (G4-FID) for establishing quadruplex-DNA affinity and selectivity of putative ligands, Bioorg. Med. Chem. Lett. 16 (2006) 4842-4845.
[113] B.T. Nguyen, E.V. Anslyn, Indicator-displacement assays, Coord. Chem. Rev. 250 (2006) 3118-3127.
[114] I. Lubitz, D. Zikich, A. Kotlyar, Specific High-Affinity Binding of Thiazole Orange to Triplex and G-Quadruplex DNA, Biochemistry 49 (2010) 3567-3574.

[115] D. Monchaud, C. Allain, M.-P. Teulade-Fichou, Thiazole orange: a useful probe for fluorescence sensing of G-quadruplex-ligand interactions, Nucleosides Nucleotides Nucleic Acids 26 (2007) 1585-1588.
[116] P. Balagurumoorthy, S.K. Brahmachari, D. Mohanty, M. Bansal, V. Sasisekharan, Hairpin and parallel quartet structures for telomeric sequences, Nucleic Acids Res. 20 (1992) 4061-4067.
[117] R. Giraldo, M. Suzuki, L. Chapman, D. Rhodes, Promotion of parallel DNA quadruplexes by a yeast telomere binding protein: a circular dichroism study, Proc. Natl. Acad. Sci. U. S. A. 91 (1994) 7658-7662.
[118] N. Berova, K. Nakanishi, R.W. Woody, Circular dichroism: principles and applications, second ed., Wiley-VCH, New York, Chichester, U.K., 2000.
[119] B. Dumat, G. Bordeau, E. Faurel-Paul, F. Mahuteau-Betzer, N. Saettel, M. Bombled, G. Metgé, F. Charra, C. Fiorini-Debuisschert, M.-P. Teulade-Fichou, *N*-phenyl-carbazole-based two-photon fluorescent probes: Strong sequence dependence of the duplex *vs* quadruplex selectivity, Biochimie 93 (2011) 1209-1218.
[120] K. Bhadra, G.S. Kumar, Interaction of berberine, palmatine, coralyne, and sanguinarine to quadruplex DNA: a comparative spectroscopic and calorimetric study, Biochim. Biophys. Acta 1810 (2011) 485-496.
[121] T. Yamashita, T. Uno, Y. Ishikawa, Stabilization of guanine quadruplex DNA by the binding of porphyrins with cationic side arms, Bioorg. Med. Chem. 13 (2005) 2423-2430.
[122] H. Sun, Y. Tang, J. Xiang, G. Xu, Y. Zhang, H. Zhang, L. Xu, Spectroscopic studies of the interaction between quercetin and G-quadruplex DNA, Bioorg. Med. Chem. Lett. 16 (2006) 3586-3589.
[123] E.W. White, F. Tanious, M.A. Ismail, A.P. Reszka, S. Neidle, D.W. Boykin, W.D. Wilson, Structure-specific recognition of quadruplex DNA by organic cations: Influence of shape, substituents and charge, Biophysical Chemistry 126 (2007) 140-153.
[124] J. Dash, P.S. Shirude, S.-T.D. Hsu, S. Balasubramanian, Diarylethynyl Amides That Recognize the Parallel Conformation of Genomic Promoter DNA G-Quadruplexes, J. Am. Chem. Soc. 130 (2008) 15950-15956.

Graphical abstract